RSC Advances

PAPER

View Article Online
View Journal | View Issue

Cite this: *RSC Adv.*, 2024, **14**, 36771

Direct dimethyl carbonate synthesis from CO_2 and methanol over a flower-like CeO_2 catalyst with 2-cyanopyridine as a dehydrating agent in continuous packed-bed reactor

Issara Sereewatthanawut,[ab] Notsawan Swadchaipong,[c] Vut Tongnan,[c] Chalempol Khajonvittayakul,[c] Panupan Maneesard,[c] Rossarin Ampairojanawong,[c] Ammarika Makdee,[c] Matthew Hartley,[d] Kang Li[e] and Unalome Wetwatana Hartley*[c]

A flower-like CeO_2 catalyst was successfully synthesized using an acrylamide graft copolymerized on glucose under hydrothermal conditions and used for the direct synthesis of dimethyl carbonate (DMC) from CO_2 and CH_3OH in a packed-bed reactor with 2-cyanopyridine as a dehydrating agent. The synthesized flower-like CeO_2 exhibited both basicity and acidity properties with values of 300 μmol g^{-1} and 80 μmol g^{-1}, respectively, according to CO_2-TPD and NH_3-TPD results. The effect of reaction parameters such as reaction temperature, feed ratio, catalyst quantity, and operating pressure on the DMC production over the flower-like CeO_2 catalyst was investigated. The optimum conditions were found to be a temperature of 120 °C, catalyst weight of 1.0 g, CH_3OH : CO_2 ratio of 1 : 1, and pressure of 30 bar, which provided the highest CH_3OH conversion, DMC selectivity, and DMC yield of 86.6%, 99.3%, and 86.0%, respectively. Furthermore, no changes were observed in the structure, morphology, and particle size of the flower-like CeO_2 catalyst after the DMC synthesis reaction, indicating that the synthesized catalyst was resistant to the reaction test under such optimum reaction conditions.

Received 27th August 2024
Accepted 31st October 2024

DOI: 10.1039/d4ra06187j

rsc.li/rsc-advances

1. Introduction

Climate change is a major issue caused by increasing carbon dioxide (CO_2) emissions into the atmosphere, and significant attention is being paid globally to reducing these emissions by converting CO_2 into value-added fuels or chemicals. The conversion of CO_2 to dimethyl carbonate (DMC) has received a lot of attention because DMC is an environmentally friendly and low toxicity chemical. DMC stands out as a remarkably versatile molecule with multifaceted chemical reactivity and serves as an exemplary green chemical methylating agent and solvent, finding wide application across various industries. It is also one of the green chemicals that is the raw material to produce electrolytes used in lithium-ion batteries due to its high dielectric constant and potential gasoline additives due to its high oxygen content and good blending properties as compared to methyl *tert*-butyl ether (MTBE).[1,2] Traditionally, DMC has been produced by several methods such as the phosgenation of methanol[3] and the oxidative carbonylation of methanol.[4] However, both procedures have significant disadvantages, such as the high toxicity of phosgene and the utilization of hazardous CO. As a result, the direct synthesis of DMC from methanol (CH_3OH) and CO_2 (reaction (1)) is considered one of the most promising ways to effectively utilize carbon resources and reduce greenhouse gas emissions, yielding just water as a byproduct.

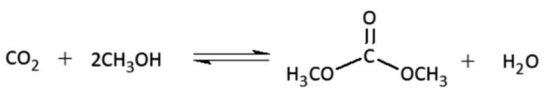

(1)

Direct DMC synthesis from CH_3OH and CO_2 is considered a green and sustainable route; however, it typically yields low amounts of DMC due to thermodynamic limitations (ΔG = +26 kJ mol^{-1}), DMC hydrolysis, and catalyst deactivation. Water removal from the reaction system is expected to shift the reaction equilibrium toward DMC synthesis resulting in enhanced DMC yield. Therefore, the catalytic activity can be boosted by water removal using several dehydrating strategies including

[a]*King Prajadhipok's Institute, Bangkok 10210, Thailand*
[b]*Faculty of Engineering and Technology, Pathumthani University, Pathumthani 12000, Thailand*
[c]*Chemical and Process Engineering, The Sirindhorn International Thai-German Graduate School of Engineering (TGGS), King Mongkut's University of Technology North Bangkok, Bangkok, 10800, Thailand. E-mail: unalome.w.cpe@tggs-bangkok.org*
[d]*Department of Chemical Engineering, Faculty of Engineering, King Mongkut's University of Technology North Bangkok, Bangkok 10800, Thailand*
[e]*Chemical Engineering, Imperial College London, SW7 2AZ, UK*

dehydration of methanol before the reaction,[5] the use of organic molecules[6] or inorganic (zeolite) materials[7] as a dehydrating agent, and the use of a membrane reactor.[8] Several studies have reported the use of different dehydrating agents such as CH_3I,[9] butylene oxide,[10] acetonitrile,[11] and 2-cyanopyridine[12–16] for water removal from the DMC synthesis reaction. Honda and co-workers[16] examined the use of various dehydrating agents for direct DMC synthesis from CH_3OH and CO_2 using CeO_2 catalyst in a batch system. They found that the use of 2-cyanopyridine as a dehydrating agent resulted in excellent catalytic activity. Moreover, 2-picolinamide product from the reaction between 2-cyanopyridine and water can be easily removed from the reaction mixture and recyclable back to 2-cyanopyridine by a dehydration reaction over a catalyst.

One of the challenges for researchers is to find suitable catalyst materials that could improve the catalytic activity for the synthesis of DMC. Generally, acid and basic sites are required for the synthesis of DMC from CO_2 and CH_3OH. CH_3OH molecules are activated at both acid and basic sites, while CO_2 molecules are adsorbed at the basic site of the catalyst. Therefore, the development of catalysts with high acidity and basicity properties are an interesting area that is currently being investigated.[3,17] So far, many studies on the direct DMC synthesis with homogeneous and heterogeneous catalysts have been published. However, homogeneous catalysts have many disadvantages such as being difficult to recycle, requiring the co-catalyst as a support to increase activity, which leads to high processing costs, as well as easily forming water as a side effect, which decomposes the catalyst and leads to deactivation.[18,19] Therefore, heterogeneous catalysts received more attention because they can overcome these disadvantages and exhibit higher stability compared to homogeneous catalysts. There are many types of metal oxides such as CeO_2, ZrO_2, SiO_2, Al_2O_3 TiO_2 and ZnO[20,21] as well as some mixed metal oxides such as CeO_2–ZrO_2, TiO_2–CeO_2, CeO_2–ZnO, ZrO_2–MgO and MgO–SiO_2[8,10,22–25] have been reported as heterogeneous catalyst for the direct DMC synthesis. Among these catalysts, cerium oxide (CeO_2) has gained a lot of attention and has become a favorable choice due to its acid–base properties, redox properties, suitable crystal structure, high oxygen storage capacity and high oxygen vacancies[26–29] which induce ability in CO_2 adsorption and CH_3OH activation led to increased catalytic activity. P. Kumar *et al.*[30] investigated the synthesis of DMC from CO_2 and CH_3OH over CeO_2 catalyst using a molecular sieve as a dehydrating agent in a batch reactor. They found that the catalytic performance was correlated with the basic and acidic properties of the CeO_2 catalyst, resulting in a DMC yield of 2.046 mmol DMC per g cat. at a reaction temperature of 120 °C, pressure of 150 bar, and reaction time of 4 h. D. Stoian *et al.*[31] studied the efficiency of the direct DMC synthesis from CO_2 and CH_3OH over the CeO_2 catalyst with the presence of 2-cyanopyridine as a dehydrating agent in both batch and continuous operations. They reported that high DMC yield was observed due to the right balance in basicity and acidity properties of CeO_2 catalyst. Furthermore, it has been reported that CeO_2 not only acts as an excellent catalyst in DMC synthesis but also in dehydration reaction of dehydrating agent (2-cyanopyridine, 2-CP) to remove water byproduct in both batch and continuous operations.[12,15]

Recently, the synthesis of CeO_2 catalyst with a special morphology such as nanorods,[32] nanotubes,[33] nanocubes,[34] nanoplates[35] and nanospheres[36] have received great attention. The different crystal facets exposed on the surface of CeO_2 nanostructures were strongly controlled by their morphologies, resulting in differential properties that can influence the interaction between the CeO_2 surface and the adsorbed reactants, as well as the catalytic performance. Wang *et al.*[28] investigated nano-CeO_2 catalysts with various morphologies (spindle, rod, cube, and octahedron) for the DMC synthesis from CH_3OH and CO_2 and found that spindle-like CeO_2 provided better catalytic efficiency than other morphologies because the spindle-like CeO_2 displayed more active (111) planes and acid–base sites, resulting in higher DMC yield. Three dimensional (3D) CeO_2 hierarchical structures, such as flower-like assembled from 1D or 2D structures, have a significant impact on performance improvements. It provided high active surface areas that facilitated surface reactions, high specific surface area and high surface-to-bulk ratio.[37–39] Moreover, CeO_2 catalyst with flower-like morphology has been rarely reported for direct DMC synthesis reaction from CH_3OH and CO_2.

Therefore, this study is interested in synthesizing a flower-like CeO_2 catalyst using a graft copolymerization reaction between acrylamide and glucose under hydrothermal treatments and applied for the direct synthesis of DMC from CO_2 and CH_3OH reaction with 2-cyanopyridine as a desiccant in a continuous tubular packed-bed reactor. The synthesized catalyst was characterized by XRD, SEM, BET, CO_2-TPD, O_2-TPD and NH_3-TPD techniques. Furthermore, the effect of reaction parameters such as temperature, feed (CH_3OH : CO_2) ratio, catalyst weight and pressure on catalytic performance for the DMC synthesis are also investigated.

2. Methodology

2.1. Catalyst preparation

A synthetic procedure is as follows: 3.6 g of glucose was dissolved in 180 mL of distilled water and stirred until completely dissolved at room temperature. 2.12 g of acrylamide and 4.34 g of cerium(III) nitrate hexahydrate were then added to the previous solution until became transparent. Subsequently, the pH of the solution was adjusted to 10–12 by adding 8–10 mL of 28–30% wt. ammonia solution and vigorously stirring. The solution was changed from a transparent solution to a viscous gel. After 5 h of continuous stirring, the brown gel was transferred to a hydrothermal bomb and stored in the oven at 180 °C for 72 h. The hydrothermal bomb was naturally cooled to room temperature. The brown suspension was washed three times with distilled water and once with ethanol using a centrifuge at 9000 rpm for 10 min before being dried overnight at 60 °C. Finally, the obtained suspension was calcined in two steps: first, at 600 °C for 12 h under Ar gas flow. Second, at 400 °C for 10 h with an air flow and a heating rate of 2 °C min^{-1}.

2.2. Catalyst characterization

The crystalline structure of the synthesized and spent catalysts were characterized using X-ray diffraction (XRD, Rigaku TTRAX III diffractometer) with Cu K_α radiation (λ = 1.5418 Å) at an accelerating voltage of 40 kV and current of 30 mA. The scanning range of 2θ was set from 20° to 90° with a step width of 0.02°. The morphology of the CeO_2 samples was investigated using Thermo Scientific Phenom Pharos G2 Desktop Field Emission Gun-Scanning Electron Microscope (FEG-SEM) with an accelerating voltage of 10 kV. Textural properties of the synthesized catalyst were studied by nitrogen physisorption technique at −196 °C using Quantachrome Autosorb-1. Prior to the measurements, the sample was degassed in vacuum to clean the catalyst surface. The specific surface area was determined using the Brunauer–Emmett–Teller (BET) method. The basicity and acidity of the synthesized catalyst were characterized using CO_2- and NH_3-temperature programmed desorption (TPD), respectively. Before starting the TPD study, the catalyst sample was packed into a quartz reactor and first pretreated at 150 °C for 1 h with a flow rate of 100 mL min^{-1} Argon gas (Ar) and then cooled to room temperature. After pretreatment, the sample was exposed to the corresponding gas mixtures at different temperatures. Individually, 100 mL min^{-1} of 5% vol. CO_2/Ar was fed at 100 °C (CO_2-TPD) or 50 mL min^{-1} of 5% vol. NH_3/Ar was fed at 50 °C (NH_3-TPD) to the system for 2 h, then cooled to room temperature by continuing the gas flow and left overnight. During the TPD process, the temperature was increased by 5 °C min^{-1} from 25 to 700 °C under Ar flow rate of 100 mL min^{-1}. The gas (CO_2 or NH_3) desorption profiles were measured using a real-time quadrupole mass spectrometer gas analyzer (GSD 320, OmniStar). O_2-temperature programmed desorption (O_2-TPD) was also measured on the above instrument. The sample (1.0 g) was first pretreated with 100 mL min^{-1} of 10% O_2/Ar at 700 °C for 1 h and then cooled to ambient temperature. After that, the sample was flushed with Ar to eliminate excess/physisorption of oxygen. The oxygen desorption amount was continuously monitored using an on-line mass spectrometer (GSD 320, OmniStar) in the presence of 100 mL min^{-1} of Ar, while the temperature was ramped up from room temperature to 800 °C at a heating rate of 5 °C min^{-1}.

2.3. Catalytic performance test

The catalytic activity of the CeO_2 catalyst for the synthesis of DMC from CH_3OH and CO_2 were evaluated by using a continuous tubular packed-bed reactor. The schematic for the DMC synthesis is shown in Fig. 1. One gram of catalyst was packed inside a stainless-steel tube between a thin layer of quartz wool (I.D. = 10 mm, O.D. = 13 mm). The heater temperature is measured by a K-type thermocouple located along the wall of the reactor near the catalyst bed and the system pressure is determined by a pressure gauge and controlled by a back pressure regulator (BPR). 2-Cyanopyridine (2-CP) as a dehydrator was dissolved in CH_3OH at a stoichiometric molar ratio (2-CP : CH_3OH = 1 : 2).[12] In the experiment, gaseous CO_2 was introduced into the reactor through a mass flow regulator to increase the pressure of the system to the desired reaction pressure. The molar feed (CH_3OH : CO_2) ratio was adjusted differently (1 : 2, 1 : 1, and 2 : 1). Separation of products is divided into two steps using 2-stage condensers. The first step captures the unwanted substance with a high boiling point (2-CP, 2-picolinamide) and the other captures the desired product substance (DMC, CH_3OH). The gas and liquid products analysis were performed by gas chromatography (Shimadzu GC-2014, FID-TCD detector).

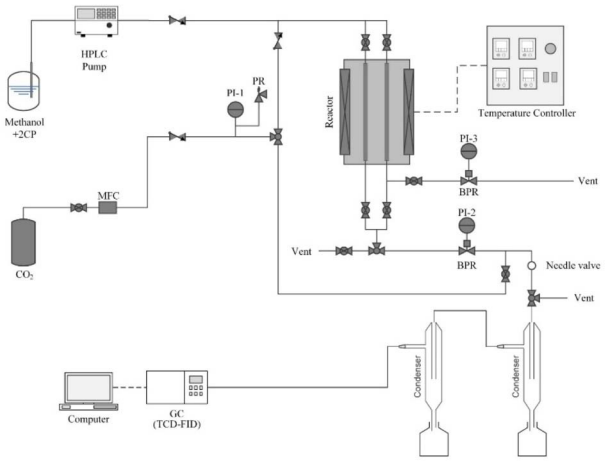

Fig. 1 Schematic illustration of the reaction system for direct synthesis of dimethyl carbonate.

3. Results and discussion

3.1. Catalyst characterizations

3.1.1. Structural analysis. The X-ray diffraction patterns of the flower-like CeO_2 catalyst before and after the reaction testing are shown in Fig. 2. The fluorite structure of CeO_2 (PDF No. 01-075-8371) was presented as a major crystalline phase in the flower-like CeO_2 catalyst before the reaction at 2θ of 28.5, 33.1, 47.5, 56.3, 59.1, 69.4, 76.7, 79.1, and 88.4°, corresponding to (111), (200), (220), (311), (222), (400), (331), (420), (422) planes, consistent with the literature.[37–39] It indicated that the calcination of the $Ce(OH)CO_3$ complex at 400 °C under air flow resulted in a complete formation of the CeO_2 structure. After

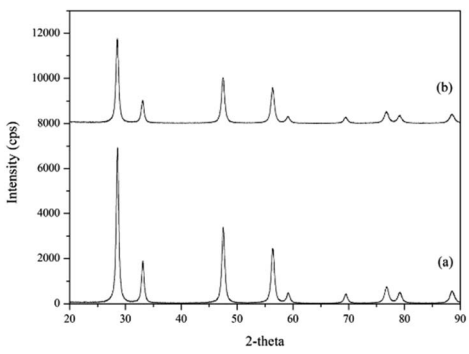

Fig. 2 XRD diffractograms of the flower-like CeO_2 catalyst: (a) before and (b) after reaction.

reaction testing, the spent flower-like CeO_2 catalyst was calcined again at 400 °C under air flow and then analyzed using XRD. The XRD patterns of the spent CeO_2 structure remained unchanged. This confirmed that the CeO_2 catalyst was resistant to the reaction test at the reaction temperature of 120 °C and reaction pressure of 10 bar. The crystallite sizes of CeO_2 before and after the reaction can be determined using the Scherrer equation, obtaining values of 16.8 and 15.6 nm, respectively. These crystallite sizes were close to Z. Zongcheng *et al.*[40] who reported crystallite sizes of flower-like CeO_2 of 15.6 nm.

3.1.2. Morphology and particle size analysis. The morphology and particle sizes of the synthesized flower-like CeO_2 catalyst prepared by hydrothermal treatments and calcined at 400 °C (before reaction) and the spent flower-like CeO_2 calcined at 400 °C (after reaction) were examined by SEM images as shown in Fig. 3 and 4, respectively. It was found that the synthesized flower-like CeO_2 in Fig. 3 appeared as three-dimensional (3D) flower-like mesoporous microspheres with a diameter of 3–4 μm. The microspheres consist of numerous petal-like plates with thickness of less than 100 nm connected to each other to form an open porous structure. Furthermore, there were no changes in the morphology and particle size of the spent flower-like CeO_2 after reaction (Fig. 4) when compared to the catalyst before the reaction (Fig. 3). This indicated that the flower-like shape of the CeO_2 catalyst was resistant to the reaction test at the reaction temperature of 120 °C and reaction pressure of 30 bar, which was consistent with the XRD data.

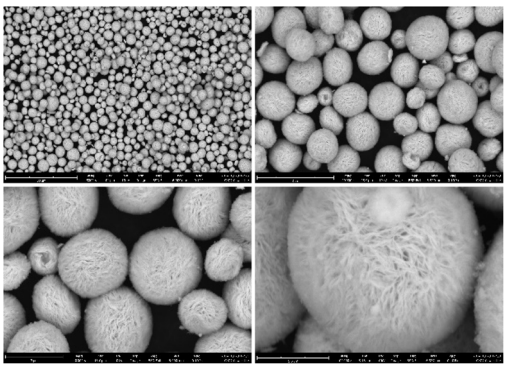

Fig. 3 SEM image of the synthesized flower-like CeO_2 catalyst (before reaction).

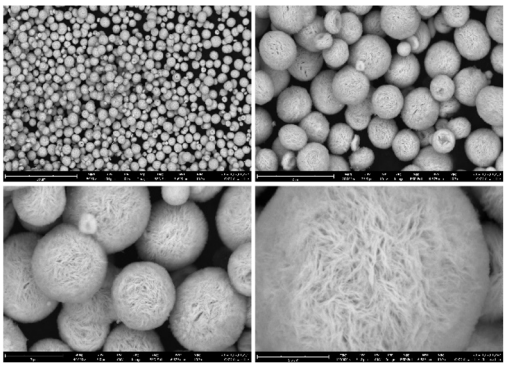

Fig. 4 SEM image of the spent flower-like CeO_2 catalyst (after reaction).

Different morphologies of CeO_2 expose distinct crystal facets on the surface, resulting in varied surface properties such as particle size, surface area, and acid–base sites, as well as differing catalytic activities. The cubic fluorite structure of CeO_2, as confirmed by XRD results, typically comprises three crystal facets: (100), (110), and (111). The surface properties of CeO_2 vary depending on these exposed facets, which have distinct oxygen vacancy formation energies, leading to varying quantities of oxygen vacancies or defects on different planes.[41,42] The synthesis of CeO_2 with different morphologies or exposed facets is influenced by the preparation conditions employed. For instance, polycrystalline CeO_2 can be prepared by the thermal decomposition of cerium nitrate,[43] which mainly terminates with the (111) surface while octahedra, rods, and cubes morphologies can be synthesized by hydrothermal synthesis.[44] The octahedra, sheets, spheres and spindle-like morphologies also expose the (111) plane while cubes expose the (100) plane and the rods consist of the (110) and (100) surfaces.[28,45–47] From Fig. 3 and 4, the flower-like structure of the CeO_2 catalyst was formed by numerous nanosheets, indicating that the observed flower-like CeO_2 exposed the (111) surface plane. Z. Zongcheng *et al.*[40] used HR-TEM to analyze the crystal facets of the flower-like CeO_2 and found lattice spacings corresponding to the (111) planes of CeO_2 which were consistent with Q. Wang *et al.*[48]

3.1.3. Porosity analysis. The N_2 adsorption–desorption isotherm as shown in Fig. 5 was used to characterize the porous properties of the synthesized flower-like CeO_2 catalyst. The synthesized catalyst exhibited a type-IV isotherm with a hysteresis loop, attributed to capillary condensation in the mesopores, indicating the presence of a mesoporous structure in the flower-like CeO_2 catalyst, which was consistent with the SEM data. The appeared hysteresis loop related to the mesoporous with tapered plate pore type with four opening sides (Fig. 5, inset). The flower-like CeO_2 catalyst had a specific BET surface area of 26.06 $m^2\ g^{-1}$. The total pore volume and average pore diameter were 0.122 $m^3\ g^{-1}$ and 93.61 Å, respectively.

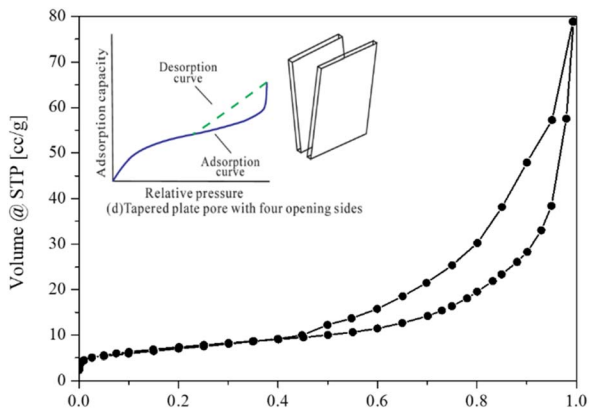

Fig. 5 N_2 adsorption–desorption isotherm of the flower-like CeO_2 catalyst and isotherm for tapered plate pore with four opening sides (inset).[49]

3.1.4. Possible mechanism of the flower-like CeO_2 microspheres formation. The flower-like CeO_2 microspheres were produced by calcining a flower-like $Ce(OH)CO_3$ microspheres twice.[50,51] The initial step was calcination at 600 °C for 12 h under inert gas to decompose $Ce(OH)CO_3$, followed by calcination at 400 °C for 10 h under air environment to oxidize Ce_2O_3 into CeO_2 structure, as described in eqn (2) and (3). The flower-like $Ce(OH)CO_3$ microspheres were synthesized *via* acrylamide graft copolymerization on glucose, with cerium(III) nitrate hexahydrate as a Cerium source. Under basic conditions, cerium salts precipitated to generate cerium hydroxide $[Ce(H_2O)_x(OH)_y]$, and acrylamide could be graft-copolymerized onto glucose to form graft-copolymers.[50] Nevertheless, in the hydrothermal process, these graft copolymers were easily decomposed, yielding many various N-containing organic molecules. As a result, a plausible formation mechanism is proposed: the created N-containing organic molecules interacted with $[Ce(H_2O)_x(OH)_y]$ particles to form $Ce(OH)CO_3$–N–R hybrids, which subsequently self-assemble to form the flower-like $Ce(OH)CO_3$ microspheres.[51]

$$2Ce(OH)CO_3 \xrightarrow{\text{decomposition}} Ce_2O_3 + 2CO_2 + H_2O \quad (2)$$

$$2Ce_2O_3 + O_2 \xrightarrow{\text{oxidation}} 4CeO_2 \quad (3)$$

3.1.5. Basicity, acidity and oxygen vacancies analysis. It has been reported that acid and basic sites presented on the surface of the catalysts have been identified as active sites for DMC synthesis from CH_3OH and CO_2. The CO_2-TPD profile as shown in Fig. 6 showed the interaction between adsorbate (gaseous CO_2) and absorbent (flower-like CeO_2) in the temperature ranges of 25–700 °C. At 100–200 °C, which is the optimum temperature for DMC synthesis, CO_2 was desorbed at low temperature and considered as weak basic site. This had a significant effect on DMC production. The calculated amount of basic site on the flower-like CeO_2 catalyst surface was 300 μmol g^{-1}. The NH_3-TPD profile of the flower-like CeO_2 catalyst in the temperature ranges of 25–700 °C is shown in Fig. 7. The desorbed NH_3 from the surface of the flower-like CeO_2 catalyst occurred in a wide peak ranging from 40 to 700 °C, corresponding to the weak, medium and strong acid site, with a total

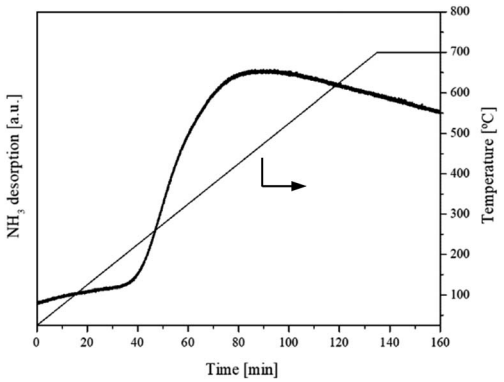

Fig. 7 NH_3-TPD profile of the flower-like CeO_2 catalyst.

NH_3 quantity of 80 μmol g^{-1}. As a result, it can be confirmed that CeO_2 catalysts have both basic and acidic sites, allowing them to behave as bifunctional acid–base catalysts. The CeO_2 catalyst surface consists of three types of surface-active sites that coexist on its surface, including (i) oxygen vacancies as redox sites, (ii) coordinately unsaturated Ce cations near the oxygen vacancies as Lewis's acid sites, and (iii) nearby oxygen ions as Lewis's basic sites.[27] The presence of oxygen vacancies within the flower-like CeO_2 catalyst was investigated using the O_2-TPD technique, as shown in Fig. 8. The O_2-TPD profile of the catalyst exhibited two desorption peaks at 400–600 °C and 600–800 °C. The lower temperature peak (400–600 °C) is attributed to desorbed oxygen that adsorbed on oxygen vacancies, which readily desorb from the surface. The higher temperature peak (600–800 °C) could be assigned to oxygen within the bulk lattice of the catalyst.[52]

3.2. Catalytic behavior

As described earlier, 2-cyanopyridine (2-CP), dissolved in CH_3OH at a 2-CP : CH_3OH molar ratio of 1 : 2, was utilized as a dehydrator to remove water from the reaction system and push the reaction equilibrium towards DMC synthesis. The hydration of 2-cyanopyridine gives 2-picolinamide (2-PA) product (eqn (4)), which is also catalyzed by the CeO_2 catalyst. The produced 2-picolinamide can be readily desorbed from the catalyst surface, easily removed from the reaction mixture and

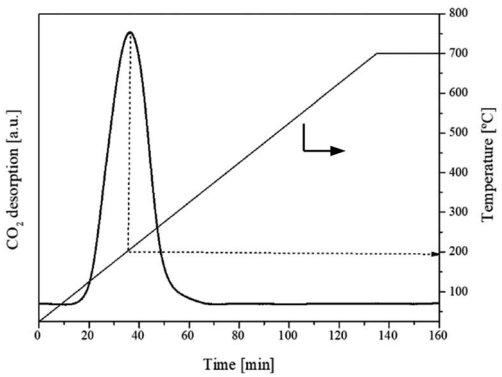

Fig. 6 CO_2-TPD profile of the flower-like CeO_2 catalyst.

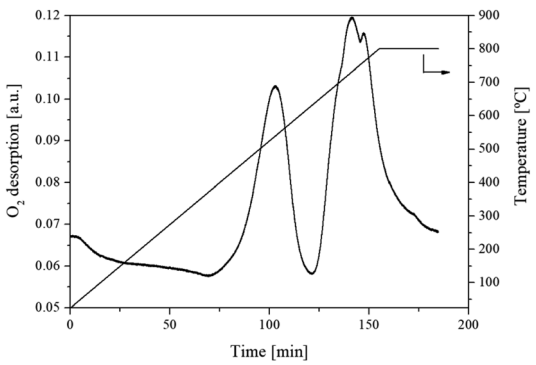

Fig. 8 O_2-TPD profile of the flower-like CeO_2 catalyst.

dehydrated to obtain 2-cyanopyridine. However, the generated 2-picolinamide can interact with CH_3OH to produce methyl picolinate (2-MP) and ammonia by-products, as shown in eqn (5).[14]

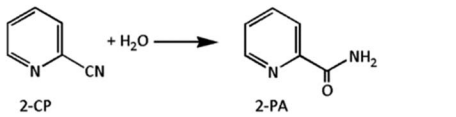

(4)

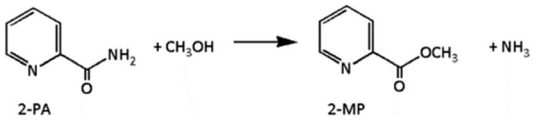

(5)

Tamura *et al.*[13] proposed a possible reaction mechanism of 2-cyanopyridine hydration by CeO_2 catalyst which can be also used to described in this work as shown in Scheme 1. The hydration occurs by dissociating H_2O to produce $H^{\delta+}$ and $OH^{\delta-}$ ions on the surface of CeO_2 catalyst (step 1). In step 2, nitrile and $Ce–OH^{\delta-}$ are in equilibrium with the nitrile – $Ce–OH^{\delta-}$ adsorption complex. In step 3, $OH^{\delta-}$ and $H^{\delta+}$ on the CeO_2 surface were attached to the cyano group of 2-CP, forming an amide (2-PA). In addition, the effects of reaction parameters such as temperature (3.2.1), feed ratio ($CH_3OH : CO_2$) (3.2.2), catalyst amount (3.2.3) and pressure (3.3.4) on the DMC production over the flower-like CeO_2 catalyst were investigated to optimize the reaction conditions.

3.2.1. Effect of reaction temperature. The influence of reaction temperature on the catalytic activity of the flower-like CeO_2 catalyst was investigated at various temperatures ranging from 100 to 140 °C (Fig. 9) while the reaction pressure, molar feed ratio and catalyst weight were 10 bar, 1 : 1 and 1.0 g, respectively. The results showed that the CH_3OH conversion, space-time yield of DMC and DMC yield increased from 32.0 to 33.9%, 15.5 to 16.4 mmol g^{-1} h and 31.8 to 32.4%, respectively, when the reaction temperature increased from 100 to 120 °C. This increase in DMC yield and CH_3OH conversion means that reactant molecules have higher kinetic energy at higher temperatures, allowing more molecules to pass the activation energy barrier and produce the products. On the contrary, the CH_3OH conversion, DMC selectivity, and DMC yield declined dramatically with further increasing operating temperature. This was primarily due to the decrease in CO_2 adsorption on the catalyst surface, as well as the increased rates of the side reactions to produce by-products such as dimethyl ether (DME) from DMC decomposition and CH_3OH dehydration, dimethoxymethane (DMM) from the reaction of CH_3OH with formaldehyde (HCHO), and methyl formate (MF) from the interaction between CH_3OH and formic acid (HCOOH) at high reaction temperatures[14,53,54] as shown in Scheme 2. Moreover, methyl carbamate (MC) was also formed at such high temperatures from the reaction between ammonia (from reaction (5)) and DMC.[14] The optimal temperature for this reaction is therefore reported at 120 °C.

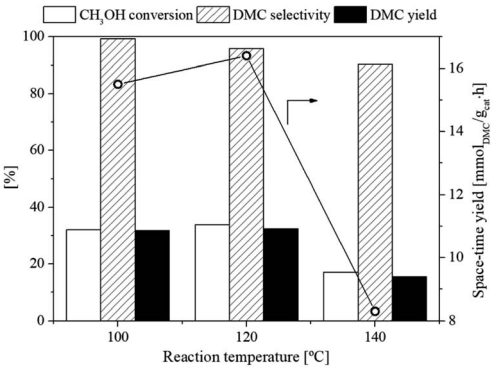

Fig. 9 Effect of reaction temperature on CH_3OH conversion, DMC selectivity, and DMC yield of the flower-like CeO_2 catalyst using 2-CP as dehydrating agent (10 bar, $CH_3OH : CO_2 = 1 : 1$).

3.2.2. Effect of feed ($CH_3OH : CO_2$) ratio. The impact of the initial molar ratio ($CH_3OH : CO_2$) on the CH_3OH conversion,

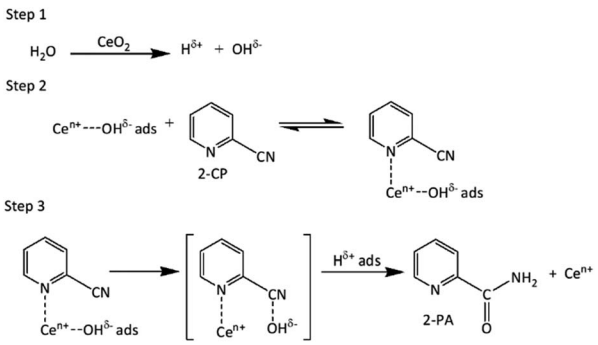

Scheme 1 Proposed reaction mechanism for the 2-cyanopyridine (2-CP) hydrolysis to form 2-picolinamide (2-PA) over the CeO_2 catalyst during the DMC synthesis from CH_3OH and CO_2.[13]

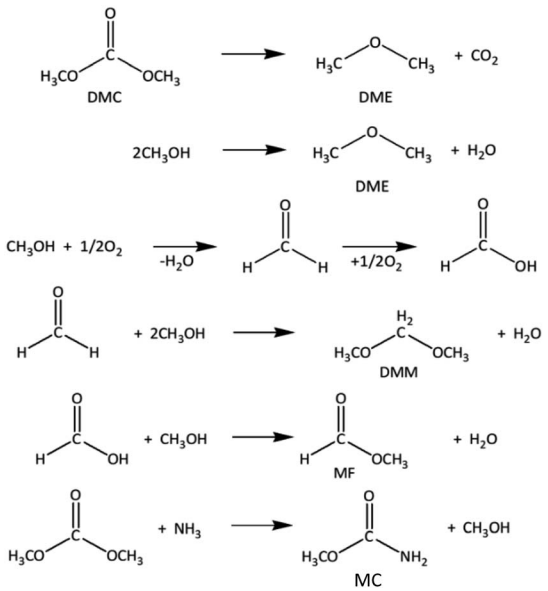

Scheme 2 Reaction of possible by-products formation during the direct synthesis of DMC from CH_3OH and CO_2 at high temperatures.[14,53,54]

DMC selectivity, and DMC yield with different feed ratios of 1 : 2, 1 : 1, and 2 : 1 was investigated. The operating temperature of 120 °C, catalyst weight of 1.0 g and pressure of 10 bar were used for this experiment. The result shown in Fig. 10 revealed that the feed ratio of 1 : 1 provided the best performance with the CH_3OH conversion, DMC selectivity, and DMC yield of 33.9, 95.8, and 32.4%, respectively. The molar ratios of 2 : 1 and 1 : 2 showed relatively lower performances possibly due to the too-high (ratio of 2 : 1) and too-low (ratio of 1 : 2) of CH_3OH concentrations reduced the reaction rate because the active sites were covered with CH_3OH (ratio of 2 : 1) or CO_2 (ratio of 1 : 2) and thus could not be accessed by another reactant in those active sites. Furthermore, the by-product DME was also produced from the CH_3OH dehydration reaction at the molar ratio of 2 : 1.

3.2.3. Effect of catalyst weight. The influence of catalyst amount on the catalytic performance of the flower-like CeO_2 catalyst for the DMC synthesis from CH_3OH and CO_2 was investigated using catalyst amounts varied at 0.5 and 1.0 g. The other experimental conditions including an operating temperature of 120 °C, a pressure of 10 bar, and a feed ratio (CH_3OH : CO_2) of 1 : 1 were chosen for this study. The results of this investigation are displayed in Fig. 11. The CH_3OH conversion, DMC selectivity, and DMC yield increased from 19.3 to 33.9%, 94.6 to 95.8%, and 18.2 to 32.4%, respectively, when the catalyst amount increased from 0.5 to 1.0 g. The observed enhancement can be described as an increase in the concentration of active sites with increasing catalyst dosage. The impact of the catalyst weight of more than 1.0 g was not examined in this work; however, excess catalyst amounts have been reported to be inefficient because of excessive active centers or mass transfer limitations that promoted the side reaction formation, resulting in significantly reduced DMC yield.[55,56]

3.2.4. Effect of reaction pressure. The influence of operating pressure on the catalytic performance of the flower-like CeO_2 catalyst for the DMC production from CH_3OH and CO_2 was investigated. Fig. 12 illustrates the CH_3OH conversion, DMC selectivity, DMC yield and space-time yield at different reaction pressures (10, 20 and 30 bar), with the reaction temperature of 120 °C, molar feed ratio of 1 : 1 and the catalyst amount of 1.0 g. The results revealed that increasing operating

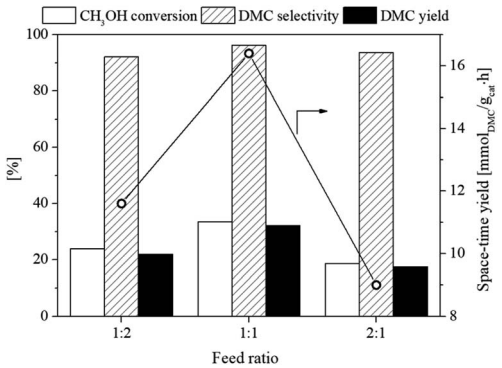

Fig. 10 Effect of feed ratio (CH_3OH : CO_2) on CH_3OH conversion, DMC selectivity, and DMC yield of the flower-like CeO_2 catalyst using 2-CP as dehydrating agent (10 bar, 120 °C).

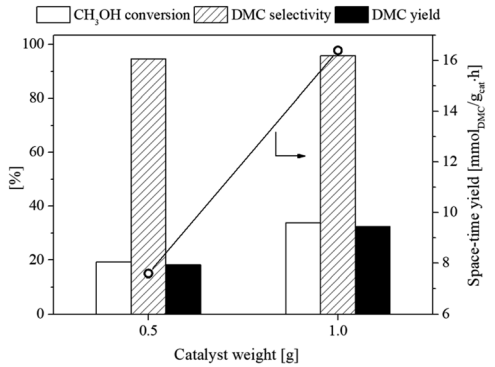

Fig. 11 Effect of catalyst contents on CH_3OH conversion, DMC selectivity, and DMC yield of the flower-like CeO_2 catalyst using 2-CP as dehydrating agent (10 bar, 120 °C, $CH_3OH : CO_2 = 1 : 1$).

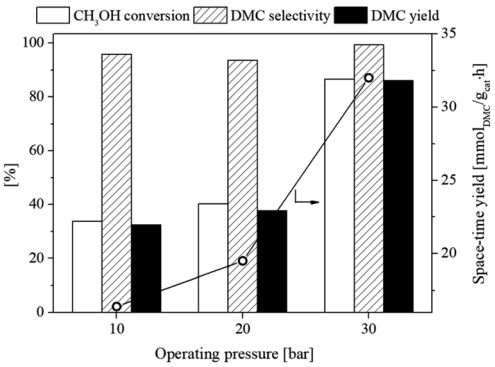

Fig. 12 Effect of operating pressure on CH_3OH conversion, DMC selectivity, and DMC yield of the flower-like CeO_2 catalyst using 2-CP as dehydrating agent (120 °C, $CH_3OH : CO_2 = 1 : 1$).

pressures from 10 to 30 bar improved CH_3OH conversion, space-time yield of DMC and DMC yield from 33.9 to 86.6%, 16.4 to 32.0 mmol g^{-1} h and 32.4 to 86.0%, respectively. This was mainly due to the ability of CH_3OH and CO_2 molecules to fully adsorb on the active sites of the catalyst resulted in a shift in chemical equilibrium towards DMC production at high operating pressures.

The results exhibited that the reaction temperature of 120 °C, catalyst weight of 1.0 g, $CH_3OH : CO_2$ ratio of 1 : 1 and operating pressure of 30 bar were the optimum conditions for the DMC synthesis using the flower-like CeO_2 catalyst, providing the highest CH_3OH conversion, DMC selectivity, and DMC yield of 86.6%, 99.3%, and 86.0%, respectively. Many works from recent years reported CeO_2 with different morphologies as one of the best catalysts for DMC synthesis, as shown in Table 1.

3.2.5. Recycling study. The reusability of the catalyst is important for their practical application. As presented in Fig. 13, the fresh flower-like CeO_2 catalyst for the DMC synthesis from CO_2 and methanol with $CH_3OH : CO_2$ molar ratio of 1 : 1 using 2-CP as dehydrating agent at temperature of 120 °C and pressure 30 bar displays CH_3OH conversion, space-time yield of DMC and DMC yield of 86.6%, 32.0 mmol g^{-1} h and 86.0%, respectively. Then, the used flower-like CeO_2 catalyst was calcined at 400 °C to remove impurity products and reactants

Table 1 Comparison of catalytic activity of the present catalyst (flower-like CeO_2) with the other reported catalysts in the direct DMC synthesis from CO_2 and CH_3OH

Catalyst	Reaction conditions	DMC yield rate ($mmol_{DMC}\ g_{cat.}^{-1}\ h^{-1}$)	Ref.
Commercial CeO_2	Fixed-bed reactor, 0.3 g catalyst, 2-CP : CH_3OH = 1 : 2, CH_3OH : CO_2 = 1 : 2.5, 30 bar CO_2, 120 °C	11.1	12
CeO_2 (calcination of $Ce(OH)_4$)	Autoclave reactor, 0.1 g catalyst, CH_3OH : CO_2 = 192 : 200 mmol, 130 °C	1.8	58
Commercial CeO_2	Autoclave reactor, 0.34 g catalyst, CH_3OH : 2-CP: = 2 : 1, 5 MPa CO_2, 120 °C	23.3	16
Spherical-CeO_2	Autoclave reactor, 0.17 g catalyst, 2-CP : CH_3OH = 1 : 1, 5 MPa CO_2, 110 °C	31.0	59
CeO_2 (calcination of $Ce(NO_3)_3 \cdot 6H_2O$) Nanorod-CeO_2 Flower-CeO_2	Autoclave reactor, 1.0 g catalyst, 742 mmol CH_3OH, 16 MPa CO_2, 250 °C	CeO_2: 2.27 Nanorod: 2.88 Flower: 3.11	60
Commercial CeO_2	Autoclave reactor, 0.34 g catalyst, CH_3OH: 2-CP = 1 : 5, 5 MPa CO_2, 120 °C	12.1	14
Spindle-CeO_2 Cube-CeO_2 Rods-CeO_2 Irregular-CeO_2	Autoclave reactor, 0.1 g catalyst, 2-CP : CH_3OH = 1 : 2, 5 MPa CO_2, 150 °C	Irregular: 79.0 Cube: 78.5 Rod: 95.5 Spindle: 152.5	57
Amorphous-CeO_2 Octahedron-CeO_2 Rod-CeO_2 Cube-CeO_2	Autoclave reactor, 0.1 g catalyst, 15 mL CH_3OH, 50 mmol 2-CP, 5 MPa CO_2, 140 °C	Amorphous: 116.9 Rod: 126.2 Octahedron: 21.8 Cube: 3.2	15
Octahedrons-CeO_2 Rods-CeO_2 Cubes-CeO_2 Spindle-CeO_2	Autoclave reactor, 0.1 g catalyst, 15 mL CH_3OH, 5 MPa CO_2, 140 °C	Octahedron: 0.35×10^{-3} Rod: 2.6×10^{-3} Cube: 1.7×10^{-3} Spindle: 4.0×10^{-3}	28
Flower-CeO_2	Packed-bed reactor, 1.0 g catalyst, 2-CP : CH_3OH : CO_2 = 1 : 2 : 1, 30 bar CO_2, 120 °C	32.0	This work

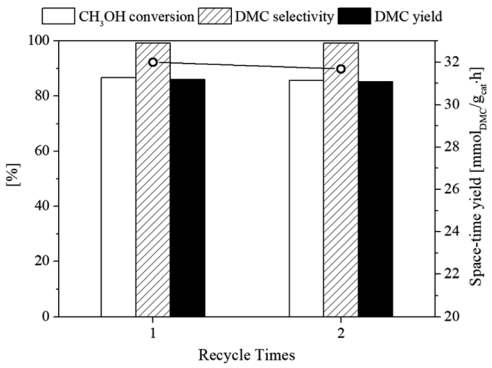

Fig. 13 Recycling of the flower-like CeO_2 catalyst for the DMC synthesis using 2-CP as dehydrating agent (30 bar, 120 °C, CH_3OH : CO_2 = 1 : 1).

on the catalyst surface before being put into the next reaction. The results showed that a significant loss of catalytic activity was not observed after two runs, indicating that the catalyst could be easily recovered.

3.3. The relationship between the catalyst properties (crystal facet and acid–base sites) and the reaction mechanism

It has been reported that the morphology, crystal facet, and acid–base sites of the catalyst were a crucial factor in achieving the highest catalytic activity for DMC synthesis. S. Wang *et al.*[28] and P. Unnikrishnan *et al.*[57] investigated the direct synthesis of DMC from methanol and CO_2 using various CeO_2 morphology catalysts. They observed that high DMC yields and methanol conversion were induced by the synergism between the exposed (111) plane, defect sites and acid–basic sites, which was controlled by CeO_2 shape. As mentioned in the morphology analysis section, the flower-like morphology of the synthesized CeO_2 catalyst indicated the (111).

Crystal facet, which was the most active plane for the DMC production from CO_2 and CH_3OH. J. Jiang *et al.*[61] performed a comprehensive study on the catalytic mechanisms of the DMC synthesis from CO_2 and methanol on CeO_2 (111) and (110) surfaces. They found that the reaction pathways computed on the (111) and (110) surfaces exhibited high catalytic activity toward DMC synthesis. However, different rate-limiting steps were observed. The rate-determining step of the (111) surface was the regeneration of oxygen vacancy *via* the dehydration process, whereas that of the (110) surface was the esterification of monomethyl carbonate (reaction (10)). The rate-limiting step on the (111) facet can be accelerated more easily than the (110) plane by using a dehydrating agent to remove water from the active site (oxygen vacancy) of the catalyst. These results suggested that the (111) facet was more reactive for DMC synthesis than the (110) facet in the presence of a desiccant. S. Wang *et al.*[28] reported that spindle-like CeO_2 produced the highest

DMC yields, followed by nanorods and nanocubes morphologies, because the spindle-like with (111) facet contained a large specific surface area, amounts of acid–basic sites and number of defect sites than nanocubes (100) and nanorods [(111) and (100)], indicating that the crystal facet of (111) plane was the active factor for the DMC formation.

It is well-known that the acidity, basicity, and redox characteristics of CeO_2 catalyst promote the CH_3OH activation and the CO_2 adsorption on its surface. The CO_2-TPD and NH_3-TPD results in Fig. 6 and 7 revealed that the synthesized flower-like CeO_2 displayed both basicity and acidity properties with amounts of 300 μmol g^{-1} and 80 μmol g^{-1}, respectively. It has been reported that both basic and acid sites activated CH_3OH molecules, however only basic sites activated CO_2 molecules, which are critical steps in the direct synthesis of DMC from CH_3OH and CO_2. The reaction mechanism of the DMC synthesis from CH_3OH and CO_2 is shown in the reaction (6)–(11).[62]

$$CH_3OH \rightarrow CH_3O_{(ads)}{}^- + H_{(ads)}{}^+ \text{ (over basic site)} \quad (6)$$

$$CO_2 \rightarrow CO_{2(ads)} \text{ (over basic site)} \quad (7)$$

$$CH_3O_{(ads)}{}^- + CO_{2(ads)} \rightarrow CH_3OCO_{2(ads)}{}^- \text{ (over basic site)} \quad (8)$$

$$CH_3OH \rightarrow CH_{3(ads)}{}^+ + OH_{(ads)}{}^- \text{ (over acid site)} \quad (9)$$

$$CH_3OCO_{2(ads)}{}^- + CH_{3(ads)}{}^+ \rightarrow (CH_3O)_2CO \quad (10)$$

$$H_{(ads)}{}^+ + OH_{(ads)}{}^- \rightarrow H_2O \quad (11)$$

In the presence of the CeO_2 catalyst, CO_2 and CH_3OH molecules are firstly adsorbed on its surface. CO_2 is adsorbed on the surface at the basic site without dissociation ($CO_{2(ads)}$) while CH_3OH is adsorbed and activated to form methoxide ions ($CH_3O_{(ads)}{}^-$) and hydrogen ions ($H_{(ads)}{}^+$) at the basic site and to form methyl ions ($CH_{3(ads)}{}^+$) and hydroxide ions ($OH_{(ads)}{}^-$) at the acid site on the CeO_2 surface. The methoxide species interacts with adsorbed CO_2 to produce methoxycarbonyl ions ($CH_3OCO_{2(ads)}{}^-$). Finally, the methoxycarbonyl ions react with methyl ions to generate dimethyl carbonate ($(CH_3O)_2CO$, DMC), while hydrogen ions react with hydroxide ions to form water (H_2O). Dimethyl carbonate and water products are desorbed from the catalyst surface, regenerating the active site. The produced H_2O can be eliminated from the reaction mixture by adding a dehydrating agent (2-cyanopyridine, 2-CP) led to an increase in the DMC yield. According to the reaction mechanism, the acidity and basicity properties of the catalyst, as well as the appearance of the (111) crystal facet in the presence of a dehydrating agent, had a significant impact on the catalytic efficiency of the DMC synthesis from CO_2 and CH_3OH.

4. Conclusions

In this study, the flower-like CeO_2 catalyst was successfully synthesized using graft copolymerization reaction between acrylamide and glucose under hydrothermal conditions. XRD and SEM results confirmed the complete formation of the flower-like CeO_2 catalyst with the crystal facet of (111) plane. When compared with the spent flower-like CeO_2 after DCM synthesis reaction, there were no changes in the structure, morphology and particle size which indicated that the flower-like CeO_2 catalyst was resistant to the reaction test at reaction temperature of 120 °C and reaction pressure of 10 bar. Furthermore, the N_2 adsorption–desorption technique revealed a mesoporous structure in the flower-like CeO_2 catalyst, which was consistent with the SEM data, with a specific BET surface area of 26.06 m^2 g^{-1}. The CO_2-TPD and NH_3-TPD results revealed that the synthesized flower-like CeO_2 displayed both basicity and acidity properties with amounts of 300 μmol g^{-1} and 80 μmol g^{-1}, respectively. The catalytic activity of the flower-like CeO_2 catalyst in producing DMC from CH_3OH and CO_2 was investigated using continuous packed-bed reactor. 2-Cyanopyridine (2-CP) was utilized as a dehydrator to remove water from the reaction system and push the reaction equilibrium toward the DMC synthesis side. The effect of reaction parameters such as temperature, feed ratio, catalyst amount and pressure on DMC production over the flower-like CeO_2 catalyst was investigated. The results exhibited that the reaction temperature of 120 °C, catalyst weight of 1.0 g, $CH_3OH : CO_2$ ratio of 1 : 1 and operating pressure of 30 bar were the optimum conditions for the DMC synthesis, providing the highest CH_3OH conversion, DMC selectivity, and DMC yield of 86.6%, 99.3%, and 86.0%, respectively. The outstanding catalytic activity of the synthesized flower-like CeO_2 catalyst for the DMC synthesis was attributed to the synergistic effect of the exposed (111) crystal plane, basicity, and acidity properties on its surface. Therefore, the catalyst could be designed to possess a suitable shape, with a mainly exposed active (111) plane, a high surface area, and a large amount of defect, basic, and acid sites, to improve catalytic performance for DMC synthesis from CO_2 and CH_3OH.

Data availability

The data that support the findings of this study are available on request.

Conflicts of interest

The authors confirm that there is no conflict of interest.

Acknowledgements

This research has received funding support from the NRCT (contract number N41A640149), King Mongkut's University of Technology North Bangkok (contract number KMUTNB-FF-66-52), and NSRF *via* the Program Management Unit for Human Resources & Institutional Development, Research and Innovation (contact number B48G660108).

References

1 D. Wang, X. Zhang, Y. Gao, F. Xiao, W. Wei and Y. Sun, *Fuel Process. Technol.*, 2010, **91**, 1081–1086.

2 T. Zhao, X. Hu, D. Wu, R. Li, G. Yang and Y. Wu, *ChemSusChem*, 2017, **10**, 2046–2052.
3 D. Delledonne, F. Rivetti and U. Romano, *Appl. Catal., A*, 2001, **221**, 241–251.
4 X. Ding, X. Dong, D. Kuang, S. Wang, X. Zhao and Y. Wang, *Chem. Eng. J.*, 2014, **240**, 221–227.
5 T. Sakakura, Y. Saito, M. Okano, J. C. Choi and T. J. Sako, *Org. Chem.*, 1998, **63**, 7095–7096.
6 J. C. Choi, K. Kohno, Y. Ohshima, H. Yasuda and T. Sakakura, *Catal. Commun.*, 2008, **9**, 1630–1633.
7 J. C. Choi, L. N. He, H. Yasuda and T. Sakakura, *Green Chem.*, 2002, **4**, 230–234.
8 C. F. Li and S. H. Zhong, *Catal. Today*, 2003, **82**, 83–90.
9 S. Fang and K. Fujimoto, *Appl. Catal., A*, 1996, **142**, 8–10.
10 V. Eta, P. Mäki-Arvela, J. Wärn, T. Salmi, J. P. Mikkola and D. Y. Murzin, *Appl. Catal., A*, 2011, **404**, 39–46.
11 M. Honda, A. Suzuki, B. Noorjahan, K. I. Fujimoto, K. Suzuki and K. Tomishige, *Chem. Commun.*, 2009, 4596–4598.
12 A. Bansode and A. Urakawa, *ACS Catal.*, 2014, **4**, 3877–3880.
13 M. Tamura, H. Wakasugi, K. I. Shimizu and A. Satsuma, *Chem.–Eur. J.*, 2011, **17**, 11428–11431.
14 M. Honda, M. Tamura, Y. Nakagawa, K. Nakao, K. Suzuki and K. Tomishige, *J. Catal.*, 2014, **318**, 95–107.
15 S. P. Wang, J. J. Zhou, S. Y. Zhao, Y. J. Zhao and X. B. Ma, *Chin. Chem. Lett.*, 2015, **26**, 1096–1100.
16 M. Honda, M. Tamura, Y. Nakagawa, S. Sonehara, K. Suzuki, K. I. Fujimoto and K. Tomishige, *ChemSusChem*, 2013, **6**, 1341–1344.
17 H. J. Lee, W. Joe and I. K. Song, *Korean J. Chem. Eng.*, 2012, **29**, 317–322.
18 D. Wang, F. Shi and L. Wang, *Catalysts*, 2024, **14**, 1–18.
19 A. Li, Y. Pu, F. Li, J. Luo, N. Zhao and F. J. Xiao, *J. CO2 Util.*, 2017, **19**, 33–39.
20 A. Kojcinovic, B. Likozar and M. Grilc, *J. CO2 Util.*, 2022, **66**, 102250.
21 N. A. M. Razali, K. T. Lee, S. Bhatia and A. R. Mohamed, *Renewable Sustainable Energy Rev.*, 2012, **16**, 4951–4964.
22 K. Tomishige and K. Kunimori, *Appl. Catal., A*, 2002, **237**, 103–109.
23 K. Tomishige, Y. Furusawa, Y. Ikeda, M. Asadullah and K. Fujimoto, *Catal. Lett.*, 2001, **76**, 71–74.
24 Z. Fu, Y. Zhong, Y. Yu, L. Long, M. Xiao, D. Han, S. Wang and Y. Meng, *ACS Omega*, 2018, **3**, 198–207.
25 K. H. Kang, C. H. Lee, D. B. Kim, B. Jang and I. K. Song, *J. Nanosci. Nanotechnol.*, 2014, **14**, 8693–8698.
26 J. Ederer, P. Janoš, M. Šťastný, J. Henych, K. Ederer, M. Š. Slušná and J. Tolasz, *J. Environ. Chem. Eng.*, 2021, **9**, 106229.
27 X. Ren, Z. Zhang, Y. Wang, J. Lu, J. An, J. Zhang, M. Wang, X. Wang and Y. Luo, *RSC Adv.*, 2019, **9**, 15229–15237.
28 S. Wang, L. Zhao, W. Wang, Y. Zhao, G. Zhang, X. Ma and J. Gong, *Nanoscale*, 2013, **5**, 5582–5588.
29 Y. Cao, H. Cheng, L. Ma, F. Liu and Z. Liu, *Catal. Surv. Asia*, 2012, **16**, 138–147.
30 P. Kumar, P. With, V. C. Srivastava, R. Gläser and I. M. Mishra, *J. Environ. Chem. Eng.*, 2015, **3**, 2943–2947.
31 D. Stoian, F. Medina and A. Urakawa, *ACS Catal.*, 2018, **8**, 3181–3193.
32 F. Meng, F. Lu, L. Wang, J. Cui and J. Lü, *Sci. Adv. Mater.*, 2012, **4**, 1018–1023.
33 G. Chen, C. Xu, X. Song, W. Zhao, Y. Ding and S. Sun, *Inorg. Chem.*, 2008, **47**, 723–728.
34 L. He, Y. Yu, C. Zhang and H. He, *J. Environ. Sci.*, 2011, **23**, 160–165.
35 H. Imagawa and S. Sun, *J. Phys. Chem. C*, 2012, **116**, 2761–2765.
36 Z. Yang, D. Han, D. Ma, H. Liang, L. Liu and Y. Yang, *Cryst. Growth Des.*, 2010, **10**, 291–295.
37 B. J. Zong, *Mater. Sci.: Mater. Electron.*, 2017, **28**, 2458–2461.
38 J. Wei, Z. Yang and Y. Yang, *CrystEngComm*, 2011, **13**, 2418–2424.
39 R. Yu, L. Yan, P. Zheng, J. Chen and X. Xing, *J. Phys. Chem. C*, 2008, **112**, 19896–19900.
40 Z. Zhan, X. Liu, H. He, L. Song, J. Li and D. Ma, *J. Rare Earths*, 2013, **31**, 750–758.
41 D. Zhang, X. Du, L. Shi and R. Gao, *Dalton Trans.*, 2012, **41**, 14455–14475.
42 M. Ziemba, C. Schilling, M. V. Ganduglia-Pirovano and C. Hess, *Acc. Chem. Res.*, 2021, **54**, 2884–2893.
43 A. Filtschew, K. Hofmann and C. Hess, *J. Phys. Chem. C*, 2016, **120**, 6694–6703.
44 H. X. Mai, L. D. Sun, Y. W. Zhang, R. Si, W. Feng, H. P. Zhang, H. C. Liu and C. H. Yan, *J. Phys. Chem. B*, 2005, **109**, 24380–24385.
45 X. Niu and F. Tu, *J. Mater. Sci.: Mater. Electron.*, 2017, **28**, 2141–2146.
46 S. Y. Yao, W. Q. Xu, A. C. Johnston-Peck, F. Z. Zhao, Z. Y. Liu, S. Luo, S. D. Senanayake, A. Martínez-Arias, W. J. Liu and J. A. P. Rodriguez, *Chem. Chem. Phys.*, 2014, **16**, 17183–17195.
47 Y. Ma, J. Liu, M. Chu, J. Yue, Y. Cui and G. Xu, *Catal. Lett.*, 2022, **152**, 872–882.
48 Q. Wang, S. Liu, S. An, X. Song, X. Liang, Z. Wang and Y. Mu, *J. Mater. Sci.: Mater. Electron.*, 2021, **32**, 26425–26438.
49 B. Xue, J. Zhang, X. Tang, C. Yang, Q. Chen, X. Man and W. Dang, *Petrochem. Res.*, 2016, **1**, 191–204.
50 C. Sun, J. Sun, G. Xiao, H. Zhang, X. Qiu, H. Li and L. Chen, *J. Phys. Chem. B*, 2006, **110**, 13445–13452.
51 H. Li, G. Lu, Q. Dai, Y. Wang, Y. Guo and Y. Guo, *ACS Appl. Mater. Interfaces*, 2010, **2**, 838–846.
52 Y. Yang, Z. Hu, K. Liu, R. Mi, D. Li, X. Yong and H. Yang, *RSC Adv.*, 2019, **9**, 4682–4692.
53 M. Álvarez, P. Marín and S. Ordóñez, *Fuel Process. Technol.*, 2023, **247**, 107805.
54 M. Yuan, M. Dong, Z. Tian, Y. Che, Y. Tian, Y. Qiao, J. Zhang and D. Li, *J. Energy Inst.*, 2022, **103**, 47–53.
55 A. H. Tamboli, N. Suzuki, C. Terashima, S. Gosavi, H. Kim and A. Fujishima, *Catalysts*, 2021, **11**, 1–16.
56 F. Wang, T. Wan, B. Da, X. Liang, N. Liu, Q. Ma, J. Xu and B. Xue, *Res. Chem. Intermed.*, 2024, **50**, 651–667.
57 P. Unnikrishnan and S. Darbha, *J. Chem. Sci.*, 2016, **128**, 957–965.
58 Y. Yoshida, Y. Arai, S. Kado, K. Kunimori and K. Tomishige, *Catal. Today*, 2006, **115**, 95–101.

59 W. Donphai, O. Phichairatanaphong, R. Fujii, P. Li, T. Chang, M. Yabushita, Y. Nakagawa and K. Tomishige, *Mater. Today Sustainable*, 2023, **24**, 100549.
60 W. Guo, L. Zheng, X. Gao, W. Yang, Y. Li, W. Sun, S. Gao, Y. Wang, X. Ding, L. Wu and T. Fang, *Appl. Catal., A*, 2023, **662**, 1–12.
61 J. Jiang, C. M. Marin, A. K. Both, C. L. Cheung, L. Li and X. C. Zeng, *Phys. Chem. Chem. Phys.*, 2021, **23**, 16150–16156.
62 K. Almusaiteer, *Catal. Commun.*, 2009, **10**, 1127–1131.